Hindawi
Advances in Civil Engineering
Volume 2023, Article ID 9953966, 14 pages
https://doi.org/10.1155/2023/9953966

Research Article

Influence of Fiber Orientation on the Shear Properties of Steel Fiber-Reinforced Reactive Powder Concrete Beams

Kejia Yang,[1] Kunliang Li ,[2] and Yiwei Lin[2]

[1]*College of Civil Engineering and Architecture, Taizhou University, Taizhou 318000, China*
[2]*College of Civil Engineering and Architecture, Wenzhou University, Wenzhou 325035, China*

Correspondence should be addressed to Kunliang Li; 1650103190@qq.com

Received 4 January 2023; Revised 9 June 2023; Accepted 3 July 2023; Published 2 September 2023

Academic Editor: Jin Luo

Steel fiber-reinforced reactive powder concrete (SFRPC) has good mechanical properties and is thus useful for engineering applications. Generally, the fibers in SFRPC are randomly distributed. To study the effects of the amount, length, and orientation of steel fibers on the shear strength of SFRPC beams, nonreinforced aligned steel fiber-reinforced reactive powder concrete (ASFRPC) beams were prepared using a large-scale electromagnetic field orientation device. Shear tests of specimens with a shear span ratio of 1.5 were performed under two fiber contents (1.0% and 2.0%) and three fiber lengths (20, 30, and 40 mm). The full-field strain during the loading process was obtained via the digital image correlation method, and the effects of fiber quantity and orientation on the shear strength of the beams were analyzed. The ASFRPC beams exhibited higher ductility but lower shear capacity than the SFRPC beams under the same conditions. The shear capacity increased with the quantity of steel fibers. According to the test results, the calculation formulas of the shear-bearing capacities of ASFRPC and SFRPC beams were established.

1. Introduction

Although concrete is a brittle material, its tensile and flexural properties are significantly improved by fiber addition [1–4]. Moreover, studies have shown that fiber has an influence on the shear capacity and shear failure characteristics of concrete members [5–10]. Xu [7] performed shear tests on 12 steel fiber-reinforced concrete (SFRC) beams without longitudinal reinforcement or stirrups and 16 SFRC beams with longitudinal reinforcement and stirrups. The test results showed that steel fiber effectively improved the shear capacity of beams, and steel fiber partially replaced the stirrups in the bending shear zone of members under certain conditions. Through tests, MEDA [8] found that the shear capacity of SFRC beams without stirrups was higher than that of concrete beams with stirrups. Beams with both stirrups and a certain amount of steel fiber exhibited greater shear strength. Majdzadeh et al. [9] compared the effects of synthetic fiber and steel fiber on the shear mechanical properties of concrete. The strengthening effect of synthetic fiber on the shear capacity of concrete members was considerably less than that of steel fiber. Slater et al. [10] collected a large number of relevant experimental results and performed theoretical analysis through two methods. Finally, a comprehensive shear strength calculation formula involving concrete matrix strength, shear span ratio, and steel fiber shape was obtained.

However, the above studies were confined to SFRC beams with random fiber orientation. Dupont and Vandewalle [11] and Wuest et al. [12] found that the fiber orientation coefficient in three-dimensional space was only ~0.45 according to the principle of stereometry. Ning [13] theoretically demonstrated that aligned SFRC members can be prepared using a magnetic field. Recently, Mu et al. [14–19] invented a fiber-based magnetic field, constructed aligned steel fiber concrete members, and performed experimental and theoretical analysis on the bending and direct shear mechanical properties of the members. The bending test results showed that the flexural strength and toughness of aligned SFRC members were 167% and 182% higher than that of SFRC members, respectively, when the water to cement ratio is 0.32. The direct shear test results showed that the shear modulus and shear strength

Table 1: Mix proportion and compression strength of RPC.

Water/binder ratio	Unit volume dosage (kg/m^3)					Compression strength f_{cu} (MPa)
	Water	Cement	Sand	Silica fume	Water reducing agent	
0.26	244.4	710.0	1266.0	230.0	3.6	82.71

Table 2: Properties of steel fibers.

Name	Diameter d_f (mm)	Length l_f (mm)	Length-to-diameter ratio (l_f/d_f)	Density (g/cm^3)	Steel fiber quantity (/kg)	Tensile strength (MPa)	Elasticity modulus (GPa)
S20	0.2	20	100		204,886		
S30	0.2	30	150	7.8	136,590	2,900	200
S40	0.2	40	200		102,840		

of aligned SFRC members were 30% and 40% higher than that of SFRC members, respectively. CECS 13 [20] and Pan et al. [21] adopted reactive powder concrete (RPC) as the matrix material because it does not contain coarse aggregate and is thus conducive to fiber rotation. The test results showed that flexural and shear strength of aligned steel fiber RPC (ASFRPC) members were 149.5% and 36.4% higher than that of steel fiber RPC members, respectively. Owing to the limitations of the internal space of the magnetic field, studies on aligned steel fiber concrete members have been limited to small-sized members.

Shear failure of structural components usually occurs at inclined sections. To investigate the shear properties of the inclined sections of aligned SFRC members, a large-scale electromagnetic field device is designed in the current study. The device was used to fabricate steel fiber-reinforced reactive powder concrete (SFRPC) and unreinforced aligned SFRPC (ASFRPC) beams with a span of 1,500 mm and cross-sectional dimensions of 160×100 mm. Through the shear test of the beam with a shear span ratio of 1.5, the relationship between the shear performance of the member and fiber distribution, quantity, and length was studied. The calculation formula of shear capacity was established according to the test results.

2. Preparation and Experimental Methods

2.1. Specimen Preparation

2.1.1. Materials. The cement used in the test was P.O.42.5R ordinary Portland cement with a packing density of 1,500 kg/m^3. The sand was river sand with with a maximum particle size of 2 mm and a fineness modulus of 2.32. The active component was silica fume with a blaine-specific surface areas of 15–27 m^2/g. The fiber was copper-plated round straight steel fibers. Polycarboxylic acid superplasticizer was used to reduce the water binder ratio of concrete. The specific proportion and cube compression strength ($150 \times 150 \times 150$ mm) are detailed in Table 1. To further reduce the rotation resistance of steel fiber in the RPC used in this test, the water-to-binder ratio of the RPC was larger than that of ordinary RPC, which also led to a lower compression strength compared with ordinary RPC. The steel fiber parameters are shown in Table 2.

2.1.2. Manufacturing Process. The large-scale electromagnetic field device shown in Figure 1(a) was used to prepare RPC beam members. The solenoid coil can generate a uniform magnetic field with an intensity of no less than 250 Gauss internally at a current of 25 A. At the same time as the magnetic field was applied, the nonmagnetic vibrating rod vibrated to make the fibers parallel to the direction of the magnetic field. As the magnetic field slid along the rail, the fiber distribution within the entire length range of the component was adjusted. Six ASFRPC beams with two volume fractions ($V_f = 1\%$ and 2%), three fiber lengths ($l_f = 20$, 30, and 40 mm), and six SFRPC beams with the same parameters were prepared using a customized large-scale electromagnetic field device. The ASFRPC and SFRPC beams contained no reinforcing rebars. The beam dimensions were $1{,}500 \times 100 \times 160$ mm. Each specimen was represented by the steel fiber length, steel fiber distribution form, and steel fiber content. Moreover, ordinary and aligned steel fiber-reinforced concretes were represented by letters R and A, respectively. For example, L20-A1.0 indicates the ASFRPC specimen with a steel fiber length of 20 mm and a fiber content of 1.0%. Because the produced ASFRPC and SFRPC beams were not reinforced, the shear capacity of the beams was far greater than the bending bearing capacity. To ensure the shear failure of the members, carbon fiber cloth was pasted at the bottom of the pure bending section of the members to prevent bending failure. The beam manufacturing photos are shown in Figure 1(b). The manufacturing flowchart is shown in Figure 2.

2.2. Shear Test

2.2.1. Test Method. The tests were designed according to the provisions in test methods used for SFRC (CECS13:2009) [20]. An electrohydraulic servo loading system was used in the experiment. The load was controlled by displacement and the loading speed was 0.5 mm/min. As shown in Figure 3, the beam span was 1,400 mm and shear span ratio was controlled to 1.5 by adjusting the position of the loading head under the distribution beam. The pressure was collected by the pressure sensor on the actuator, and the displacement of the test specimen was collected by the displacement sensors arranged at the loading point, midspan, and support. The strain nephogram of the beam surface was measured using image analysis method, which is introduced in the following

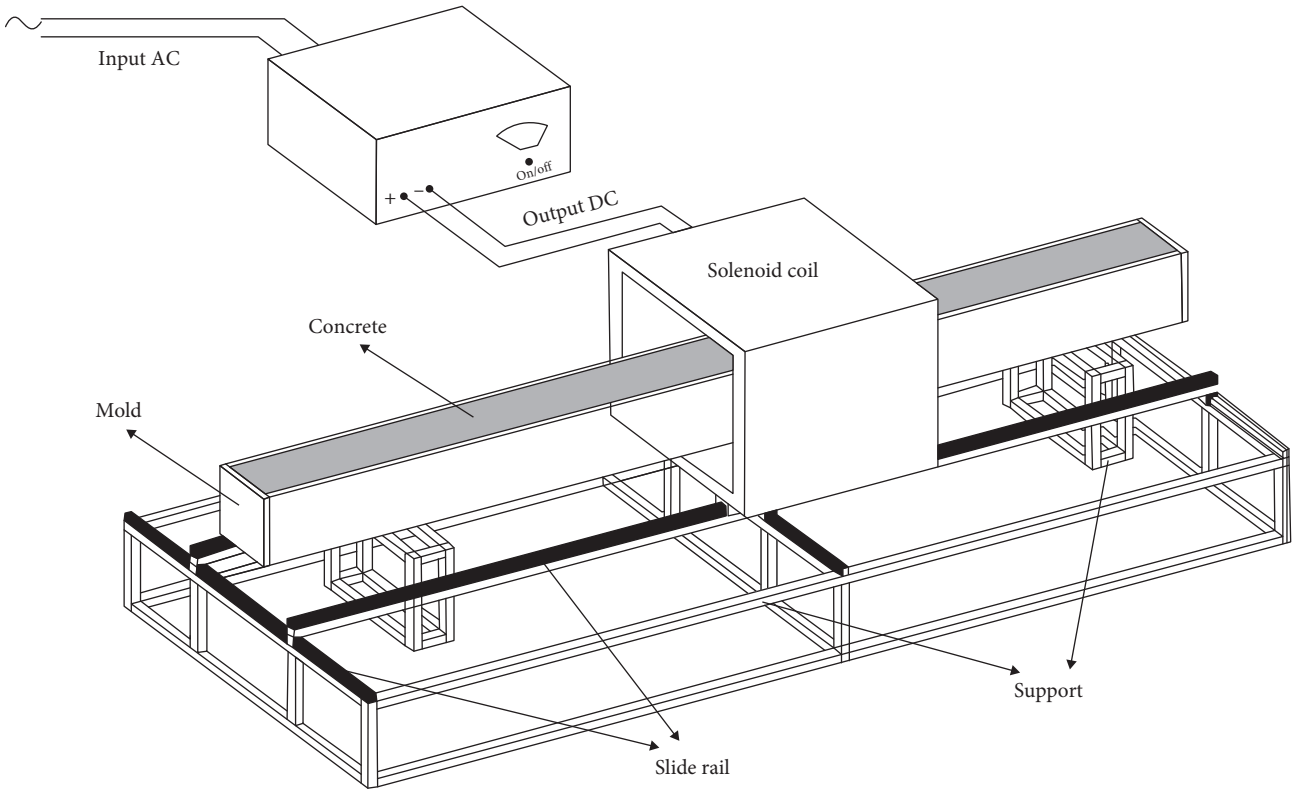

(a)

(b)

Figure 1: Electromagnetic field device and specimen manufacture process. (a) Schematic of the large magnetic field equipment. (b) Specimen manufacture photos.

section. To avoid flexural failure, two layers of carbon fiber cloth were pasted at the bottom of the pure bending section of the beam.

2.2.2. Image Analysis Method. To meet the digital image correlation (DIC) analysis requirements, the observation surface of the component needs to be processed. First, the observation surface was sprayed with a white primer (Figure 4). After the painted surface was dry, black speckles were applied to the surface with a marker pen. Because of the uncertainty associated with shear cracks, it was necessary to deposit the black speckles on the whole bending shear area of the beam. Through the DIC method, the full-field strain information on the whole bending shear section surface during loading can be analyzed, and the relative displacement between any two or more points on the observation surface can be obtained.

During image analysis via the DIC method, the coordinate information on a certain reference plane was obtained through size calibration. When the specimen is subjected to a load, it will undergo corresponding deformation (including tension, compression, and translation); therefore, the original reference plane will also undergo corresponding deformation. Because the speckle coordinates will correspondingly change after deformation, the displacement information on the reference area can be obtained through mathematical methods [21, 22]. For example,

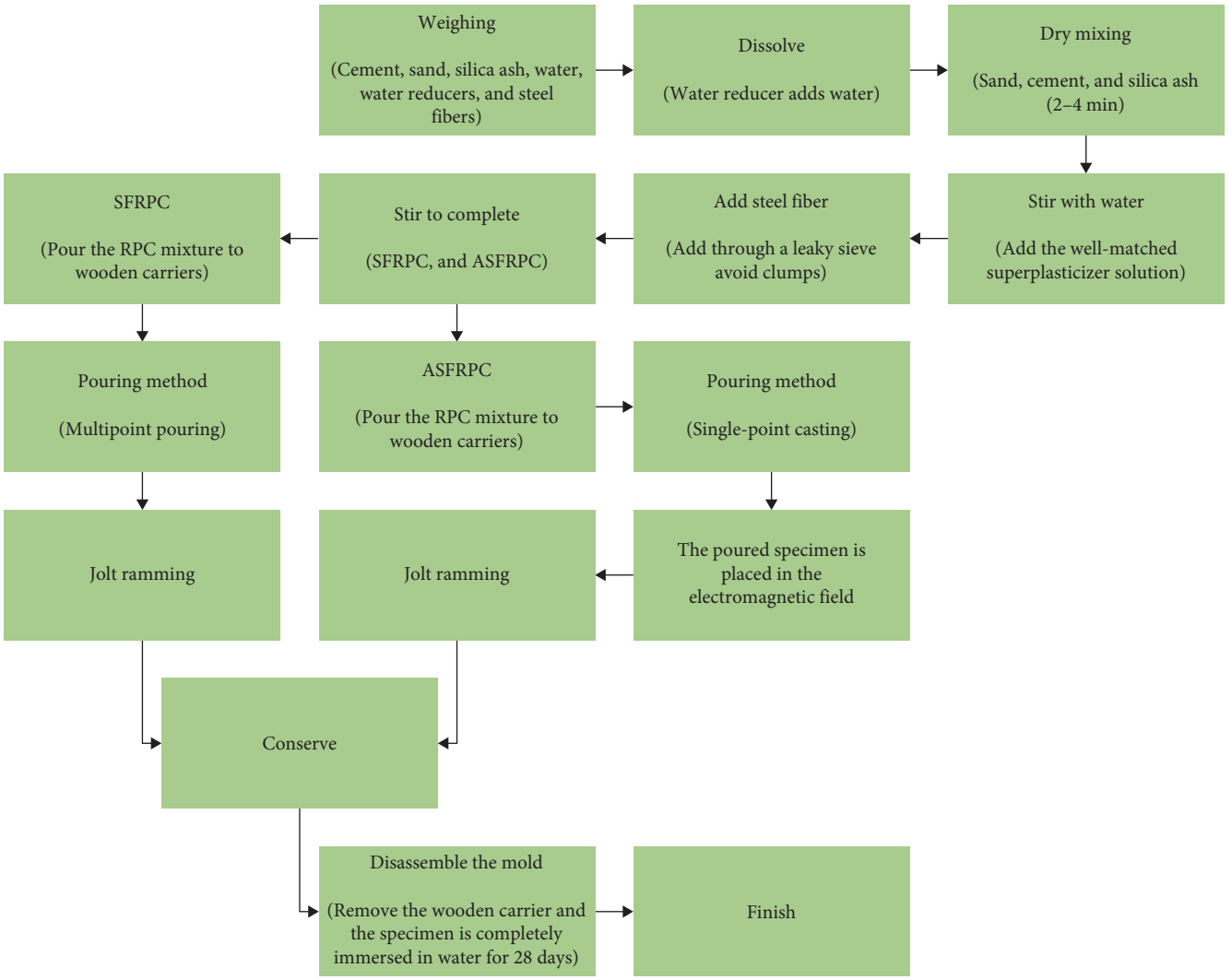

Figure 2: Flowchart of specimen production.

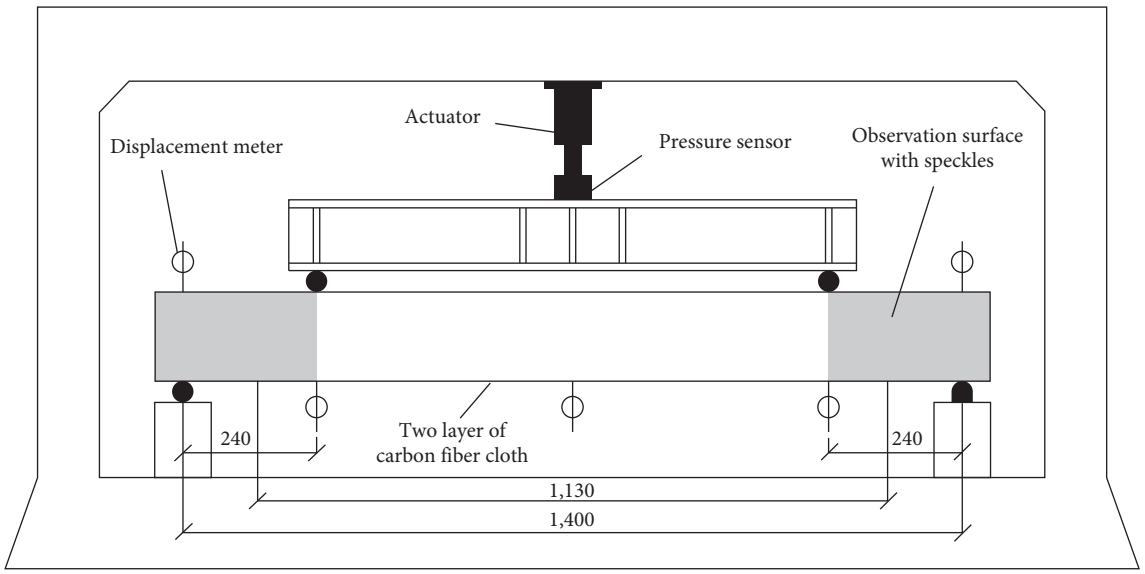

Figure 3: Schematic of loading device.

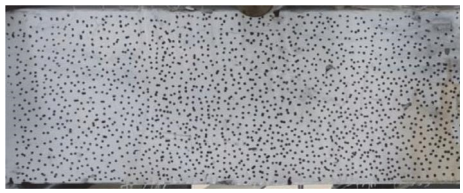

Figure 4: Treatment of observation surface.

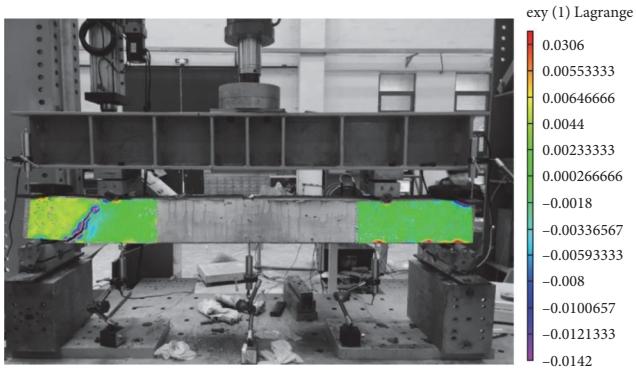

Figure 5: Measured strain cloud map of the L20-A1% beam (as an example).

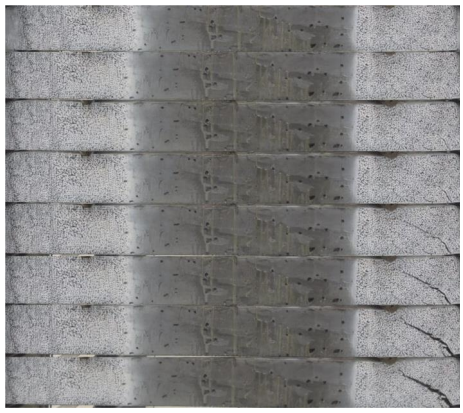

Figure 6: Failure mode and crack form of the L30-A1% ASFRPC beam (as an example).

the strain cloud in the y-direction of the bending shear zone when the L20-A1% beam was damaged was obtained via the DIC method (Figure 5).

3. Test Phenomenon and Data Processing

3.1. Shear Failure Mode. Figure 6 shows crack occurrence and development in the bending shear zone of the L20-A1% beam with increasing loading. Oblique shear cracks were generated from the vicinity of the supports. With increasing loading, the cracks developed obliquely upward along the 45° direction and continued to widen. A few fine oblique cracks occurred in the same direction around the main crack. After the peak load was reached, the oblique crack finally extended to the loading point above the beam, the width of the main crack increased rapidly after penetration, and the bearing capacity of the specimen decreased rapidly, which marked the final shear failure of the specimen. As the bearing capacity of the beam decreased rapidly after cracking, the other uncracked end of the beam will also be unloaded; therefore, failure only occurred at one end.

3.2. Test Data Processing. Twelve unreinforced beams were tested, and the load, strain, and displacement information in the shear failure process was collected. The steel fiber content, fiber direction, fiber length, section size, shear span ratio, peak load, midspan displacement, and loading point displacement of each beam are shown in Table 3.

4. Analysis of Test Results

4.1. Load–Displacement Curves. Figures 7(a) and 7(b) are the load–midspan displacement curves of ASFRPC and SFRPC beams, respectively. The load–midspan displacement curve of the beams under shear loading was linear at the initial loading stage, which indicated that no significant slip occurred between the steel fiber and the matrix at this stage, and good coordination existed between the fiber and the matrix. The initial stiffness of beams increased with the increase in fiber volume fraction, which ranged from 38 to 18 kN/mm. With increasing load, the curve gradually deviated from linearity, and microcracks and slips occurred between steel fiber and concrete. The ASFRPC and SFRPC beams showed the same change trend before reaching the ultimate load. After the load peak, the main crack occurred. At this time, all of the SFRPC beams rapidly lost their bearing capacity, and the load–displacement curves showed brittle failure characteristics. Although the bearing capacity of the ASFRPC beams also rapidly decreased, the beams could maintain a certain bearing capacity within a certain displacement range. The load–displacement curves showed plastic characteristics, and the longer the steel fiber, the more significant the plastic characteristics. By comparing Figures 7(a) and 7(b), it can be seen that the peak displacements of SFRPC specimens were 11.4%–69% larger than that of the ASFRPC specimens with the same parameters. This was mainly due to the larger embedded length of fibers perpendicular to the inclined section in the SFRPC specimens.

Fiber volume fraction is the most stable and significant influencing factor on the shear bearing capacity. The shear bearing capacities of all the specimens increase with the increase in fiber volume fraction. Unlike the flexural specimens, the shear bearing capacity of ASFRPC beams were lower than that of the SFRPC beams. For the specimens with the fiber volume fraction of 1%, the shear bearing capacity of ASFRPC beams were 22.8%–27.2% lower than those of the SFRPC beams. For the specimens with the fiber volume fraction of 2%, the shear bearing capacity of ASFRPC beams were 14.1%–30.1% lower than those of the SFRPC beams. Fiber length also has a certain impact on shear bearing capacity. Under the same fiber content, the longer the fiber, the smaller the number of fibers, resulting in lower shear bearing capacity. When the fiber length increased from 20 to 30 mm, the reduction in bearing capacity ranged from

Table 3: Summary of test results.

Sample type	Specimen variable (%)	Sectional dimension b(mm)	h(mm)	Shear span ratio λ	V_u(kN)	Δ_1(mm)	Δ_2(mm)	Δ_3(mm)
SFRPC	L20-R1	100	160	1.5	79.4	3.40	8.45	5.74
	L30-R1	100	160	1.5	75.5	5.07	8.99	5.21
	L40-R1	100	160	1.5	65.7	6.57	11.2	6.81
	L20-R2	100	160	1.5	89.5	5.62	8.50	5.35
	L30-R2	100	160	1.5	82.9	5.76	9.89	5.31
	L40-R2	100	160	1.5	78.1	5.98	10.44	5.52
ASFRPC	L20-A1	100	160	1.5	61.3	5.61	6.74	3.70
	L30-A1	100	160	1.5	52.9	3.89	6.72	3.71
	L40-A1	100	160	1.5	47.8	6.78	7.98	3.77
	L20-A2	100	160	1.5	76.9	5.05	7.57	5.02
	L30-A2	100	160	1.5	58.2	3.48	6.45	4.12
	L40-A2	100	160	1.5	54.6	3.31	7.05	4.43

*Δ_1 is the displacement of the right loading point; Δ_3 is the displacement of the left loading point; Δ_2 is the midspan displacement.

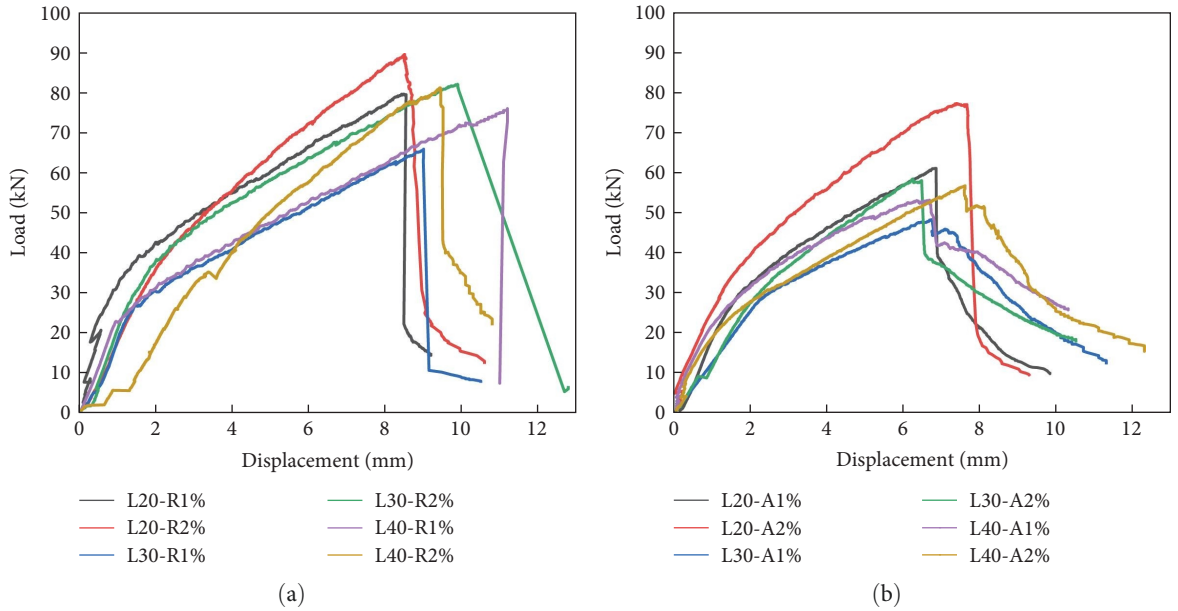

Figure 7: Load–midspan displacement curve. (a) SFRPC beam and (b) ASFRPC beam.

5.2% to 7.4% for SFRPC specimens and 13.7% to 24.3% for ASFRPC specimens. When the fiber length increased from 30 to 40 mm, the reduction in bearing capacity ranged from 5.8% to 13.0% for SFRPC specimens and 6.2% to 9.6% for ASFRPC specimens.

Unlike reinforced concrete beams, the shear failure of ASFRPC and SFRPC beams only occurred at one end. We extracted the loading point displacement at the failure end of the beam and plotted the load-failure end displacement curves of SFRPC and ASFRPC beams, as shown in Figures 8(a) and 8(b). As can be seen from Figure 8, the ultimate displacement at the failure end of SFRPC and ASFRPC beams had no obvious relationship with the length and content of steel fibers, and the ultimate displacements at the failure of all random steel fiber concrete beams were basically the same.

Taking L30-R2% and L30-A2% as examples, Figures 9(a) and 9(b) show the curves of load versus three displacements (Δ_1, Δ_2, and Δ_3) of ASFRPC and SFRPC beams, respectively. The displacements at the first two loading points of the peak load were similar. After the peak load, because failure occurred at one end, and unloading occurred at the other end, the displacement of one side increased, and the displacement of the other side remained unchanged or even decreased. The midspan displacement before the peak was much larger than the displacement at the loading point, and the displacement at the failure end after the peak gradually exceeded the midspan displacement.

4.2. Strain Analysis. Taking L30-A2% as an example, Figure 10 shows the y-direction strain cloud diagram of the bending

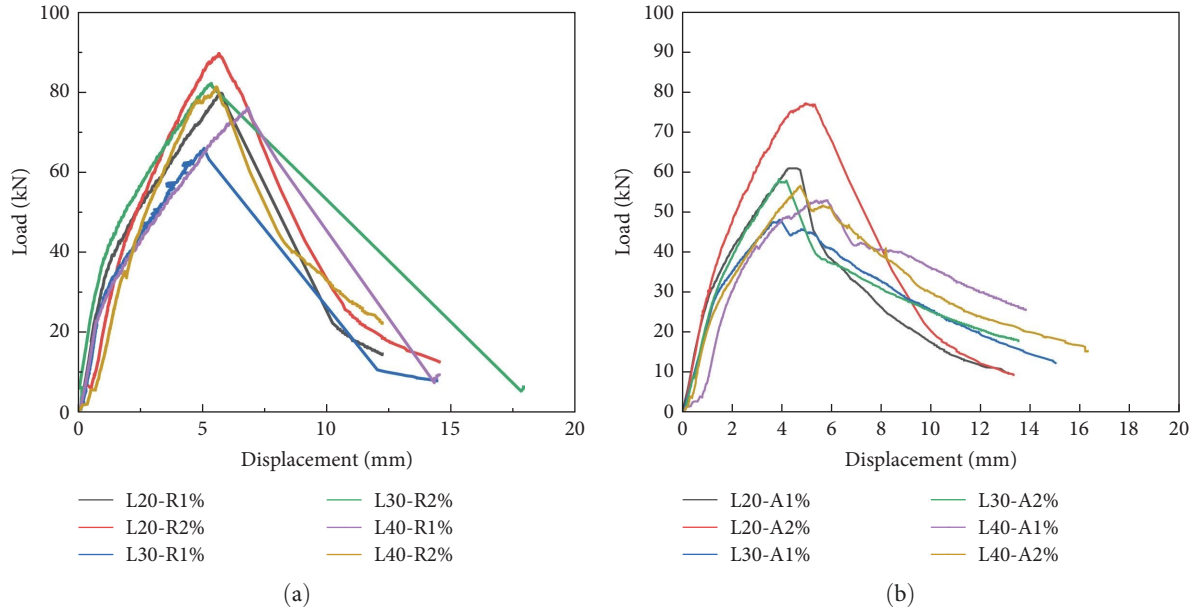

Figure 8: Load–displacement curve at the failure end. (a) SFRPC beam and (b) ASFRPC beam.

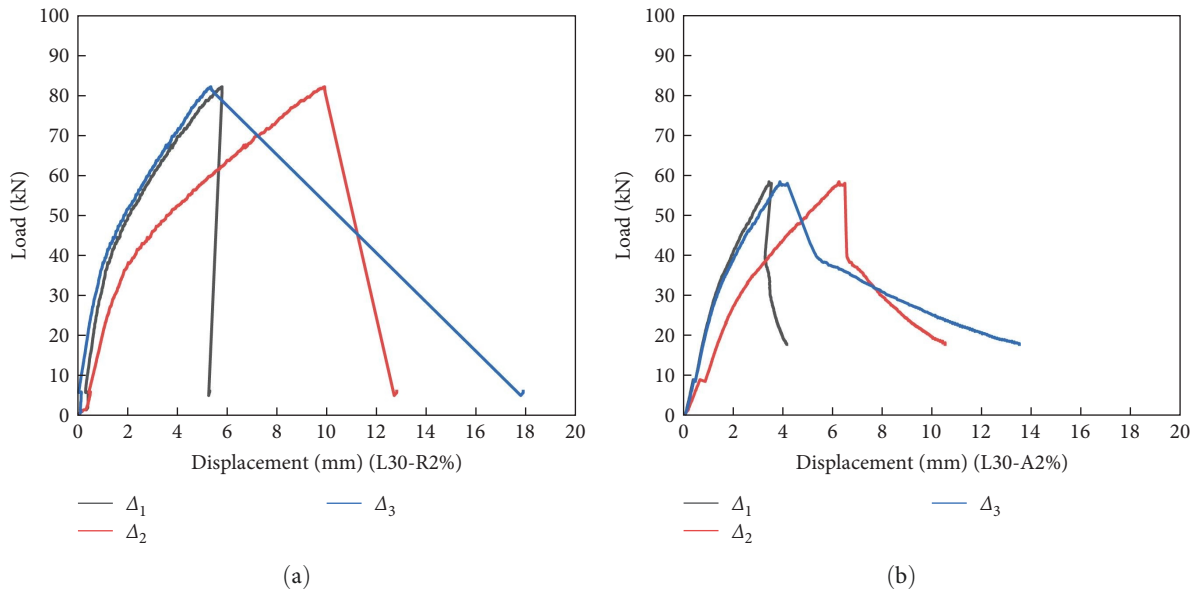

Figure 9: Load–displacement curves of three measuring points. (a) SFRPC beam and (b) ASFRPC beam.

Figure 10: Full-field strain cloud map for different loading stages (L30-A2%).

shear zone of the beam at different loading stages. At small loading, the strain in the bending shear zone was relatively uniform, except for a large local strain at the bearing and loading point. With increasing loading, the strain in the bending shear zone of the beam gradually increased, and several strain-concentration zones were gradually formed in the 45° oblique direction, which were also potential shear cracks. With the continuous increase in the load until the peak load was reached, the strain near one of the potential inclined cracks increased significantly, which indicates that the main crack occurred and that the crack width developed rapidly. With the development of the main crack, the stress of the matrix on both sides was relieved. Therefore, except for the main crack, the rest of the strain rebounded to a certain extent.

A virtual strain gauge was used to measure the average strain of the component surface in a given range (usually circular). As shown in Figure 10, virtual strain Gauges A and B were arranged in two potential cracking areas to measure the strain. Before cracking, the average strains of A and B increased with increasing load. With the formation of the main crack at Point B, the strain at Point B increased significantly, while the adjacent strain at Point A decreased. Taking components with the fiber volume fraction of 2% as examples, the load versus average strain curves for Points A and B are shown in Figure 11(a)–11(f). The components with fiber volume fraction of 1% exhibited similar phenomena.

4.3. Shear Capacity

4.3.1. Influence of Fiber Quantity. Figure 12 is a bar chart showing the relationship between the shear capacity of ASFRPC and SFRPC beams and fiber length and content. Figure 13(a) is the data chart of the shear capacity of SFRPC beams. The figure shows that at a steel fiber content of 1%, the shear capacity of beams with a fiber length of 20 mm was 5.2% higher than that of beams with a fiber length of 30 mm. The shear capacity of the beam with a fiber length of 30 mm was 13.0% higher than that of the beam with a fiber length of 40 mm. At a steel fiber content of 2%, the shear capacity of the beam with a fiber length of 20 mm was 7.4% higher than that of the beam with a fiber length of 30 mm, and the shear capacity of the beam with a fiber length of 30 mm was 5.8% higher than that of the beam with a fiber length of 40 mm. The bearing capacity data of ASFRPC beams followed a similar trend (Figure 13(b)).

The above phenomenon is attributable to the number of fibers. The shear capacity of a beam depends on the tensile capacity at the inclined crack, which is directly related to the fiber bridging effect at the crack. Therefore, under the same fiber content and distribution, the longer the fiber, the fewer the fibers at the crack, and the lower the shear capacity.

4.3.2. Influence of Fiber Distribution. To facilitate the analysis of the influence of the steel fiber direction on the shear capacity of the beam, the curves of the relationship between shear capacity and fiber direction were constructed (Figure 12). As shown in Figure 12(a), at a fiber content of 1%, the shear capacities of ASFRPC beams with fiber lengths of 20, 30, and 40 mm were 22.8%, 29.9%, and 27.2% lower than those of the corresponding SFRPC beams, respectively. As shown in Figure 12(b), at a fiber content of 2%, the shear capacities of ASFRPC beams with fiber lengths of 20, 30, and 40 mm were 14.1%, 29.1%, and 30.1% lower than those of the corresponding SFRPC beams, respectively. Because the steel fibers in the ASFRPC beam were distributed parallel to the member axis, but the angle between the shear crack and the axial direction of the member was ~45°, the bridging effect of the fibers in the direction perpendicular to the crack was lower than that of the SFRPC beam. Therefore, under the same conditions, the shear-bearing capacities of all ASFRPC beams were lower than those of the SFRPC beams.

4.4. Calculation Formula of Shear Capacity

4.4.1. Shear Capacity of SFRPC Beam. Because there was no reinforcement in the beams in the test, and the influencing factors included the fiber distribution direction, there is no applicable formula. According to the technical specification for fiber-reinforced concrete structures (CECS38:2004) [23] and equations proposed by Narayanan and Darwish [24], the ultimate shear strength of SFRC beams consists of two parts: concrete and fiber, which can be calculated using Equations (1)–(3). Equation (1) is calculated as follows:

$$v_{\mathrm{u}} = e\left(0.24 f_{\mathrm{spfc}} + 80\rho/\lambda\right) + 1.7015F, \tag{1}$$

where $v_{\mathrm{u}} = V_{\mathrm{u}}/bh$, is the ultimate shear strength of the SFRC beam; ρ is the longitudinal reinforcement ratio; λ is the shear span ratio (at $\lambda > 2.8$, $e = 1.0$, and at $\lambda \leq 2.8$, $e = 2.8/\lambda$); and f_{spfc} is the cylinder splitting strength of the concrete, which can be calculated using Equation (2):

$$f_{\mathrm{spfc}} = f_{\mathrm{CUF}}/\left(20 - \sqrt{F}\right) - 0.7 + \sqrt{F}, \tag{2}$$

where f_{CUF} is the compressive strength of a cube concrete test block with a side length of 100 mm. In the above equation, F is the fiber coefficient, which is calculated using Equation (3):

$$F = \left(l_f/d_f\right) V_f D_f, \tag{3}$$

where D_f is a parameter related to the fiber shape. For straight fiber, corrugated fiber, and concave fiber, $D_f = 0.5$, 0.75, and 1, respectively.

For the SFRPC, the f_{spfc} can still be calculated using Equation (2), and the f_{spfc} computing process for SFRPC is shown in Table 4.

Studies have found that the length-to-diameter ratio of steel fibers and fiber quantity affected the strength of SFRC beams [15–17, 25]. Because beams in the test did not contain reinforcement, the stress in the compression zone of the section was considerably lower than that of the reinforced beam when shear failure occurred, which resulted in a lower shear capacity of the member compared with that of the reinforced beam. The e value in Equation (1) according to the original formula will lead to the larger calculated shear capacity of concrete. Considering the above reasons and the simplicity of the formula, e was taken as 1 in this study. The shear capacity of SFRPC beams can be calculated using Equation (4):

$$v_u = 0.24 f_{\mathrm{sfpc}} + f(N), \tag{4}$$

where $f(N)$ is the shear strength provided by steel fibers, which is a function of N, and N is a parameter jointly determined by fiber quantity and length-to-diameter ratio.

The $f(N)$ value can be obtained by substituting the measured v_u and the calculated f_{sfpc} into Equation (4). At

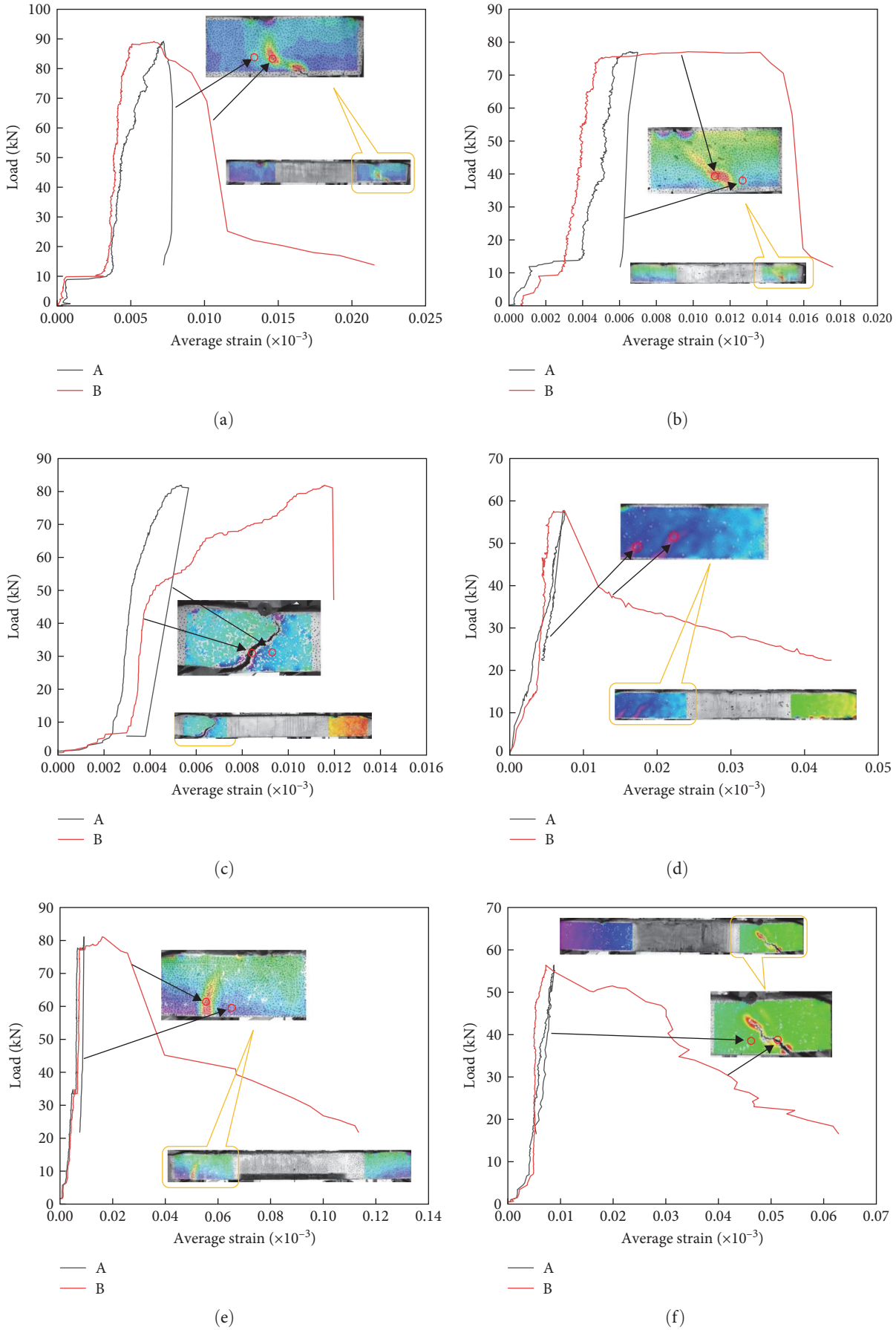

Figure 11: Load versus average strain curves for components with the fiber volume fraction of 2%. (a) L20-R2%, (b) L20-A2%, (c) L30-R2%, (d) L30-A2%, (e) L40-R2%, and (f) L40-A2%.

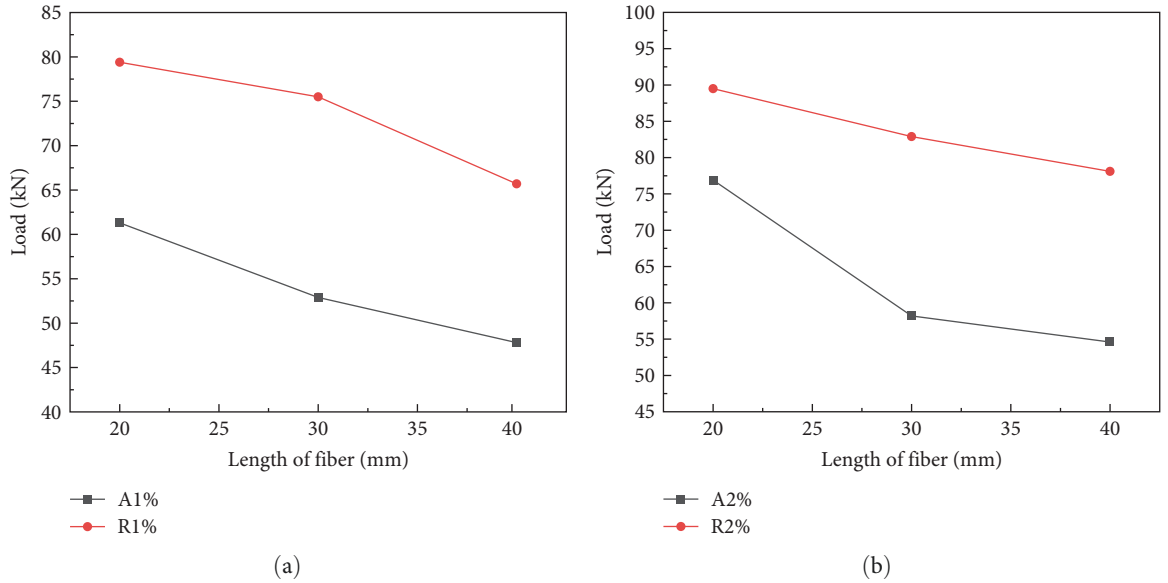

Figure 12: Relationship curves of shear capacity versus fiber direction. (a) Fiber content 1% and (b) fiber content 2%.

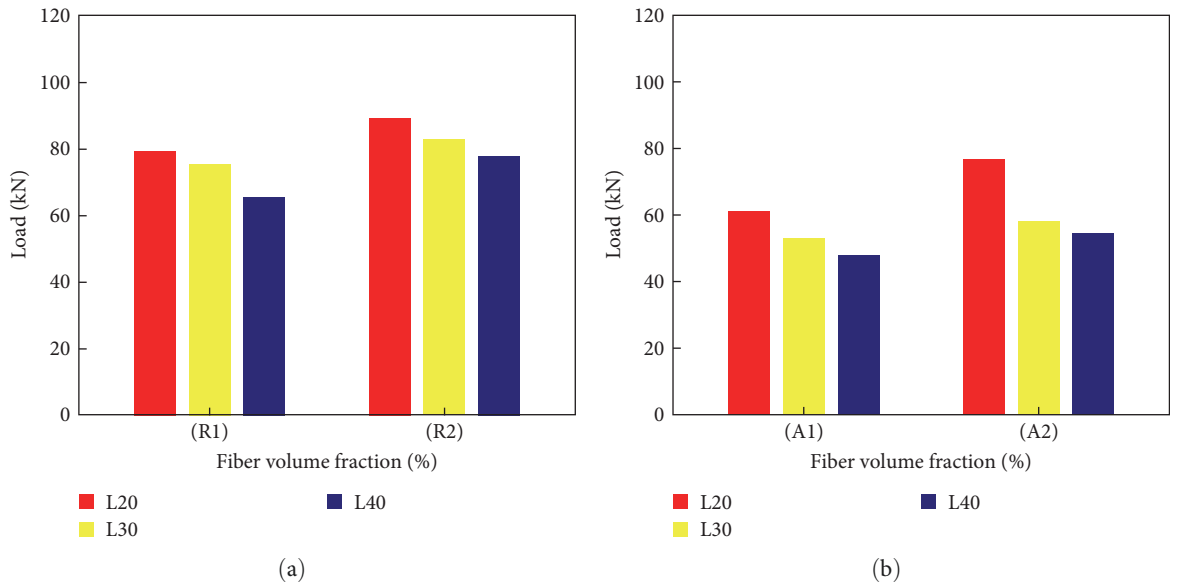

Figure 13: Comparison of shear-bearing capacities of ASFRPC and SFRPC beams. (a) SFRPC beam and (b) ASFRPC beam.

$l_f = 20$ mm and $V_f = 1\%$, the relative quantity of fibers Q_{rfq} is set to 1. The relative quantity of fibers in other proportions can be calculated using Equation (5). The parameters calculated according to the test results of SFRPC are shown in Table 5. Equation (5) is calculated as follows:

$$Q_{rfq} = 2000\, V_f / l_f, \tag{5}$$

where V_f is fiber volume fraction, and l_f is fiber length.

Figure 14 shows the fitting results for the case in which only the relative quantity of fibers is considered and $N = Q_{rfq}$. The calculation result has an approximate linear relationship, but the scatter error of the fitting straight line is large.

To further reduce the error of the fitting function, the influence of the fiber length-to-diameter ratio is introduced. N is determined by the relative fiber number Q_{rfq} and the function n, which is related to the fiber length-to-diameter ratio; that is, $N = Q_{rfq} + n$. Through trial calculations, Equation (6) and the corresponding expression Equation (7) are obtained for n and N, respectively. At this time, the function obtained by fitting was Equation (8). The relationship between the calculated scattered points and the fitting straight line is shown in Figure 15. The sum of squares of the fitting

Table 4: Computing process of f_{spfc} for SFRPC.

Sample type	The specimen variable (%)	l_f/d_f	λ	F	f_{cu}(N/mm^2)	f_{CUF}(N/mm^2)	f_{sfpc}(N/mm^2)
SFRPC	L20-R1	100	1.5	0.5	82.71	87.06	4.52
	L30-R1	150	1.5	0.75	82.71	87.06	4.72
	L40-R1	200	1.5	1	82.71	87.06	4.88
	L20-R2	100	1.5	1	82.71	87.06	4.88
	L30-R2	150	1.5	1.5	82.71	87.06	5.16
	L40-R2	200	1.5	2	82.71	87.06	5.40

Table 5: Parameters calculated according to test results of SFRPC.

Sample type	The specimen variable (%)	Measured value v_u(N/mm^2)	0.24f_{sfpc} (N/mm^2)	$f(N)$ (N/mm^2)	Length dianeter ratio l_f/d_f	Relative fiber number Q_{rfq}
SFRPC	L20-R1	2.481	1.085	1.395	100	1
	L30-R1	2.356	1.133	1.213	150	0.67
	L40-R1	2.05	1.171	0.879	200	0.5
	L20-R2	2.794	1.171	1.623	100	2
	L30-R2	2.588	1.238	1.350	150	1.33
	L40-R2	2.444	1.296	1.148	200	1

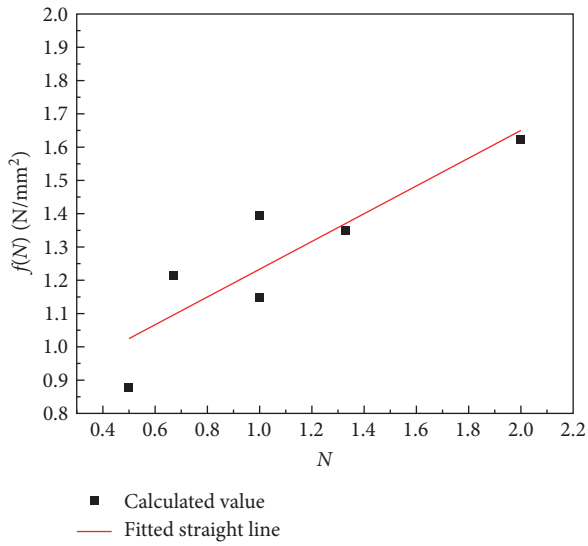

Figure 14: Straight line fitting with variable $N = Q_{rfq}$.

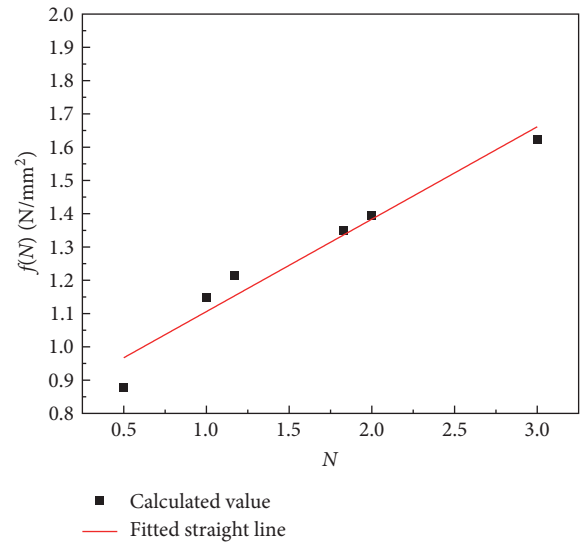

Figure 15: Straight line fitting with variable $N = Q_{rfq} + n$.

residuals after adjustment is only 0.01489, which is relatively small.

$$n = -\frac{l_f}{100d_f} + 2, \tag{6}$$

$$N = Q_{rfq} - \frac{l_f}{100d_f} + 2, \tag{7}$$

$$f(N) = 0.27768\,N + 0.82834. \tag{8}$$

The shear strength of SFRPC beams is calculated using Equation (9), which can be obtained by substituting Equation (7) into Equation (8):

$$v_u = 0.24\,f_{sfpc} + 0.27768\left(Q_{rfq} - \frac{l_f}{100d_f} + 2\right) + 0.82834, \tag{9}$$

where v_u is the shear strength; Q_{rfq} is the relative fiber quantity; l_f is the fiber length; d_f is the fiber diameter.

Table 6 compares the measured and calculated v_u values. The measured average v_u value is $\sum v_u/n = 2.452$, the standard deviation is 0.0521, and the relative standard deviation is only 2.12%. Therefore, it is feasible to calculate the shear capacity of SFRPC beams using Equation (9).

Table 6: Calculated value of v_u and its evaluation.

Sample type	Specimen variable (%)	l_f/d_f	f_{sfpc}(N/mm^2)	Q_{rfq}	v_u(N/mm^2)		Error value	Standard deviation
					Calculated	Measured		
SFRPC	L20-R1	100	4.52	1	2.4685	2.481	0.0125	0.0521
	L30-R1	150	4.72	0.67	2.2860	2.356	0.07	
	L40-R1	200	4.88	0.5	2.1384	2.05	0.0884	
	L20-R2	100	4.88	2	2.8325	2.794	0.0385	
	L30-R2	150	5.16	1.33	2.5749	2.588	0.0131	
	L40-R2	200	5.40	1	2.4020	2.444	0.042	

Table 7: Computing process of correction factor C.

Sample type	The specimen variable (%)	Measured value v_{au}(N/mm^2)	$0.24f_{sfpc}$ (N/mm^2)	$Cf(N)$ (N/mm^2)	$f(N)$ (N/mm^2)	C
ASFRPC	L20-A1	1.916	1.085	0.831	1.3843	0.6007
	L30-A1	1.653	1.133	0.520	1.152	0.451
	L40-A1	1.494	1.171	0.323	0.9674	0.3339
	L20-A2	2.403	1.171	1.232	1.6615	0.7415
	L30-A2	1.819	1.238	0.571	1.3369	0.4271
	L40-A2	1.706	1.296	0.410	1.106	0.3707

4.4.2. Shear Capacity of ASFRPC Beam. The test results showed that the shear capacities of the ASFRPC beams decreased in varying degrees compared with those of the SFRPC beams with the same fiber length and content. The steel fibers aligned in the direction perpendicular to the inclined crack had a smaller projection length compared with the randomly distributed fibers and thus exhibited a reduced bridging effect at the crack. Theoretically, the shear strength formula of the ASFRPC beam can be obtained by adjusting the fiber-provided shear strength in Equation (9). Therefore, a correction factor C is introduced into Equation (9) to obtain the formula for calculating the shear strength of ASFRPC beams (Equation 10). According to the test results, the correction factor C can be calculated as shown in Table 7.

$$v_{au} = 0.24\, f_{sfpc} + Cf(N). \tag{10}$$

Considering that steel fiber alignment only changed the projection length of steel fibers in the direction perpendicular to the crack but did not change the relative fiber quantity, C is fitted with the length-to-diameter ratio to obtain a linear relationship as shown in Figure 16.

The correction factor C is calculated using Equation (11). The shear strength calculation equation can be obtained by substituting Equation (11) into Equation (10), as shown in Equation (12).

$$C = -0.3188\frac{l_f}{100d_f} + 0.96568, \tag{11}$$

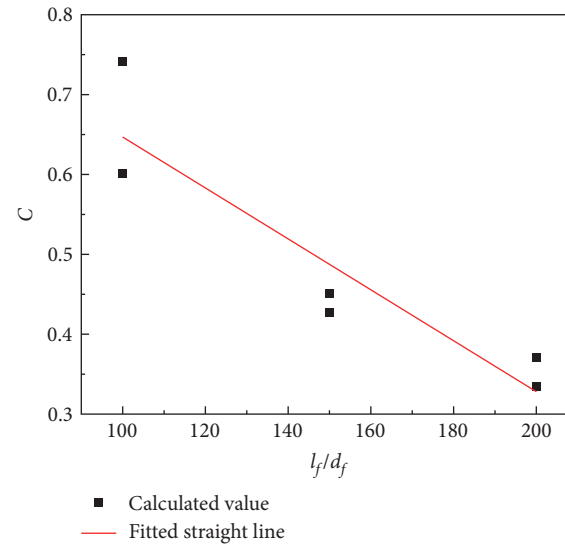

Figure 16: Fitting curve for C.

$$v_{au} = 0.24f_{sfpc} + \left(-0.3188\frac{l_f}{100d_f} + 0.96568\right)f(N). \tag{12}$$

Table 8 compares the measured and calculated v_{au} values. The measured average value of v_{au} is $\sum v_{au}/n = 1.711$, the standard deviation is 0.0951, and the relative standard deviation is only 5.5%. Therefore, it is feasible to calculate the shear capacity of SFRPC beams using Equation (12).

Table 8: Calculated value of v_{au} and its evaluation.

Sample type	The specimen variable (%)	f_{sfpc}(N/mm^2)	l_f/d_f	$f(N)$ (N/mm^2)	v_{au}(N/mm^2)		Error value	Standard deviation
					Calculated	Measured		
ASFRPC	L20-A1	4.52	100	1.3843	1.9797	1.916	0.0637	0.0951
	L30-A1	4.72	150	1.152	1.6948	1.653	0.0418	
	L40-A1	4.88	200	0.9674	1.4886	1.494	0.0054	
	L20-A2	4.88	100	1.6615	2.2460	2.403	0.1570	
	L30-A2	5.16	150	1.3369	1.8901	1.819	0.0711	
	L40-A2	5.40	200	1.106	1.5689	1.706	0.1371	

5. Conclusions

(1) The shear strength of SFRPC beams was significantly affected by the fiber quantity. Under the same steel fiber content, with increasing steel fiber length, the quantity of steel fibers decreased, and the shear capacity of the beams decreased.

(2) When shear failure occurred, the angle between the diagonal crack and the axial direction of the member was ∼45°, and the bridging effect of randomly distributed steel fibers in the direction perpendicular to the crack was greater than that of aligned steel fibers; consequently, the SFRPC beams exhibited a higher shear capacity than the ASFRPC beams under the same conditions.

(3) Shear failure occurred only at one end of the beam, and ASFRPC beams exhibited higher ductility than SFRPC beams. The longer the fiber, the more significant the ductility at beam failure.

(4) With increasing loading, the strain in the bending shear zone gradually concentrated toward the potential diagonal cracks. At ultimate loading, a diagonal crack occurred, and the strain across the crack was significantly increased. Moreover, the matrix on both sides was unloaded, causing shear failure of the beam.

(5) According to the test results and existing related research, the shear strength calculation formula of SFRPC beams related to fiber number and fiber length-to-diameter ratio was obtained through data fitting. The shear capacity formula of ASFRPC beams was obtained through modification of the steel fiber part of the shear strength formula. The formulas presented in this paper agreed well with the experimental results.

Data Availability

The data that support the findings of this study are available from the corresponding author upon reasonable request.

Conflicts of Interest

The authors declare that they have no conflicts of interest.

References

[1] P. Rossi, P. Acker, and Y. Malier, "Effect of steel fibres at two different stages: the material and the structure," *Materials and Structures*, vol. 20, pp. 436–439, 1987.

[2] Y. Du, Y. Aoyu, and Q. Honghui, "Fiber reinforced high strength concrete heat burst study," *Journal of Building Materials*, vol. 24, no. 1, pp. 216–223, 2021.

[3] A. M. Brandt, "Fibre reinforced cement-based (FRC) composites after over 40 years of development in building and civil engineering," *Composite Structures*, vol. 86, no. 1–3, pp. 3–9, 2008.

[4] R. F. Zollo, "Fiber-reinforced concrete: an overview after 30 years of development," *Cement and Concrete Composites*, vol. 19, no. 2, pp. 107–122, 1997.

[5] K. Rashid and N. Balouch, "Influence of steel fibers extracted from waste tires on shear behavior of reinforced concrete beams," *Structural Concrete*, vol. 18, no. 4, pp. 589–596, 2017.

[6] D. H. Lee, S.-J. Han, K. S. Kim, and J. M. LaFave, "Shear capacity of steel fiber-reinforced concrete beams," *Structural Concrete*, vol. 18, no. 2, pp. 278–291, 2017.

[7] X. Xu, *Experimental Study on Shear Capacity of Steel Fiber Reinforced Concrete Members*, Southwest Jiaotong University, Chengdu, China, 2018.

[8] A. Meda, F. Minelli, G. A. Plizzari, and P. Riva, "Shear behaviour of steel fibre reinforced concrete beams," *Materials and Structures*, vol. 38, pp. 343–351, 2005.

[9] F. Majdzadeh, S. M. Soleimani, and N. Banthia, "Shear strength of reinforced concrete beams with a fiber concrete matrix," *Canadian Journal of Civil Engineering*, vol. 33, no. 6, pp. 726–734, 2006.

[10] E. Slater, M. Moni, and M. Shahria Alam, "Predicting the shear strength of steel fiber reinforced concrete beams," *Construction and Building Materials*, vol. 26, no. 1, pp. 423–436, 2012.

[11] D. Dupont and L. Vandewalle, "Distribution of steel fibres in rectangular sections," *Cement and Concrete Composites*, vol. 27, no. 3, pp. 391–398, 2005.

[12] J. Wuest, E. Denarie, and E. Baruhwiler, "Determination of fiber distribution and orientation in fiber reinforcrd composites," *Exper Technol*, vol. 33, no. 5, pp. 50–55, 2009.

[13] C. Ning, "Discussion on possibility of directional steel fiber reinforced concrete," *Prestressing Technology*, vol. 92, no. 3, pp. 8–10, 2012.

[14] R. Mu, X. Qiu, and Q. Zhao, "Unidirectional distributed steel fiber reinforced cement matrix composites (I): direction control of steel fiber," *Journal of Building Materials*, vol. 18, no. 2, pp. 208–213, 2015.

[15] R. Mu, H. Li, and X. Wang, "Unidirectional distributed steel fiber reinforced cement matrix composite (ii): preparation

and strengthening effect of steel fiber," *Journal of Building Materials*, vol. 18, no. 3, pp. 387–392, 2015.

[16] R. Mu, C. Wang, and H. Li, "One-way distribution of steel fiber reinforced cement matrix composites (III): fracture," *Journal of Building Materials*, vol. 19, no. 1, pp. 78–82, 2016.

[17] R. Mu, C. Diao, H. Liu et al., "Design, preparation and mechanical properties of full-field aligned steel fiber reinforced cementitious composite," *Construction and Building Materials*, vol. 272, Article ID 121631, 2021.

[18] R. Mu, H. Li, L. Qing, J. Lin, and Q. Zhao, "Aligning steel fibers in cement mortar using electro-magnetic field," *Construction and Building Materials*, vol. 131, pp. 309–315, 2017.

[19] R. Mu, Z. Wang, X. Wang, L. Qing, and H. Li, "Experimental study on shear properties of aligned steel fiber reinforced cement-based composites," *Construction and Building Materials*, vol. 184, pp. 27–33, 2018.

[20] CECS 13, *Test Methods Used for Steel Fiber Reinforced Concrete*, China Association for Engineering Construction Standardization, Beijing, China, 2009.

[21] B. Pan, K. Qian, H. Xie, and A. Asundi, "Topical review: two-dimensional digital image correlation for in-plane displacement and strain measurement: a review," *Measurement Science & Technology*, vol. 20, no. 6, pp. 152–154, 2009.

[22] B. Pan, H. Xie, Z. Guo, and T. Hua, "Full-field strain measurement using a two-dimensional Savitzky–Golay digital differentiator in digital image correlation," *Optical Engineering*, vol. 46, no. 3, Article ID 033601, 2007.

[23] H. Chengkui and Z. Guofan, "Technical specification for fibre concrete structure (CECS38: 2004) introduction," *Building Structure*, vol. 04, pp. 74–79, 2005.

[24] R. Narayanan and I. Y. S. Darwish, "Use of steel fibers as shear reinforcement," *ACI Structural Journal*, vol. 84, no. 3, pp. 216–227, 1987.

[25] A. R. Khaloo and N. Kim, "Influence of concrete and fiber characteristics on behavior of steel fiber reinforced concrete under direct shear," *ACI Materials Journal*, vol. 94, no. 6, pp. 592–601, 1997.